Lattice setup for quantum field theory in AdS_2

Richard C. Brower,[1,2,*] Cameron V. Cogburn,[1,†] A. Liam Fitzpatrick,[1,‡] Dean Howarth,[1,§] and Chung-I Tan[3,‖]

[1]*Department of Physics, Boston University, Boston, Massachusetts 02215-2521, USA*
[2]*Center for Computational Science, Boston University, Boston, Massachusetts 02215, USA*
[3]*Brown Theoretical Physics Center and Department of Physics, Brown University, Providence, Rhode Island 02912-1843, USA*

(Received 2 October 2020; accepted 14 April 2021; published 14 May 2021)

Holographic conformal field theories (CFTs) are usually studied in a limit where the gravity description is weakly coupled. By contrast, lattice quantum field theory can be used as a tool for doing computations in a wider class of holographic CFTs where nongravitational interactions *in AdS* become strong, and gravity is decoupled. We take preliminary steps for studying such theories on the lattice by constructing the discretized theory of a scalar field in AdS_2 and investigating its approach to the continuum limit in the free and perturbative regimes. Our main focus is on finite sublattices of maximally symmetric tilings of hyperbolic space. Up to boundary effects, these tilings preserve the triangle group as a large discrete subgroup of AdS_2, but have a minimum lattice spacing that is comparable to the radius of curvature of the underlying spacetime. We quantify the effects of the lattice spacing as well as the boundary effects, and find that they can be accurately modeled by modifications within the framework of the continuum limit description. We also show how to do refinements of the lattice that shrink the lattice spacing at the cost of breaking the triangle group symmetry of the maximally symmetric tilings.

DOI: 10.1103/PhysRevD.103.094507

I. INTRODUCTION

Our expectations about what kinds of behavior are possible in physical systems are often strongly affected by the tractable examples we have at our disposal. Conformal field theories (CFTs) suffer from the disadvantage that finding examples to work with can be difficult since one has to make sure that all β functions vanish. Consequently, known classes of CFTs tend to be fairly rigid in that they have at most a small number of discrete parameters.

By contrast, one of the strengths of AdS/CFT is that the conformal symmetry of the field theory dual is built into the spacetime isometries of the AdS description for any values of the bulk parameters, so the boundary theory is automatically conformal. If one is content to work with effective theories in AdS, one can thereby easily scan over large classes of CFTs with many continuously tuneable parameters. These classes can be a fantastic source of concrete models for many types of strongly coupled physics, and in many cases have eventually led to a deeper understanding of the behavior in the field theory which can after the fact be formulated without reference to a bulk dual. However, these classes of bulk models are still rather special because in order to be calculationally tractable, the bulk theory usually must be taken to be perturbative.[1] We will refer to such theories as "large N" CFTs, where N is not necessarily related to the central charge of the CFT but rather refers to the fact that all correlators are Gaussian to leading order in a small expansion parameter "$1/N$".

To go beyond the class of weakly coupled bulk theories, one would like to be able to do strong coupling calculations in AdS. The best-developed numeric tool for QFT at strong coupling is lattice field theory, and by applying it to strongly coupled QFTs *in AdS* one can potentially learn about qualitatively new kinds of CFTs. An initial objection might be that it is not clear how to include gravity in a lattice calculation, and therefore the CFT duals would not contain a stress tensor. However, we can nevertheless consider such theories as "nonlocal" CFTs that satisfy most of the usual axioms of conformal field theory (e.g., crossing symmetry, associative operator product expansion,

*brower@bu.edu
†cogburn@bu.edu
‡fitzpatr@bu.edu
§howarth@bu.edu
‖chung-i_tan@brown.edu

[1]See [1] for interesting work on bulk theories that are calculable due to large N *in the bulk* rather than due to weak coupling. See also [2–4].

invariance of correlators under the global conformal algebra, etc.), minus the existence of a stress tensor. Perhaps more intuitively, decoupling gravity in the bulk theory can be thought of as taking the limit of an infinite central charge c the boundary theory; under what conditions it is possible to actually realize such theories as the large c limit of a sequence of finite c theories is an interesting open question. Even with gravity decoupled, the theories we consider will still be "small N" in that correlators of generic operators will not be approximately Gaussian.

The goal of this paper is to build the basic lattice scaffolding to do these nonperturbative calculations in AdS. We will restrict our attention to the case of AdS_2, though in principle it should be possible to work in any number of dimensions. The first step in constructing a lattice field theory is to choose a lattice that respects as well as possible the isometries of the target manifold and to understand the UV and IR cut-off effects, which are referred to as lattice spacing and finite volume errors, respectively. Both of these are more challenging and novel in hyperbolic space than in flat space.

On two-dimensional manifolds of constant curvature, the triangle group provides an elegant approach to maintaining a maximal discrete subgroup of the AdS_2 isometries. The approach is essentially to choose a fundamental triangle and generate the lattice by reflection on the edges. For example a familiar case in flat space is that starting with an equilateral triangle, one generates the infinite triangulated lattice. In negative curvature hyperbolic space, there are an infinite number of such tessellations, some of which are illustrated in the classic Escher drawings. These hyperbolic graphs play a role in tensor networks [5–7] and quantum error correction codes [8,9] in the context of AdS/CFT. Additionally, hyperbolic lattices have recently been realized in circuit QED experiments experimentally [10] and theoretically [11]. As such, we present a sketch of the triangle group algebra with the hope of relevance beyond the present context.

The main difference with tilings of flat space is that in hyperbolic space, there is a minimum possible size of the triangles in units of the spatial curvature, i.e., the lattice spacing cannot be taken arbitrarily small while preserving the full discrete subgroup of spatial symmetries. Consequently, in order to use lattice methods to probe distances shorter than the AdS curvature length ℓ, we must subdivide ("refine") our maximally symmetric lattice in a way that breaks the discrete symmetries. Nevertheless, the maximally symmetric lattices are useful for several reasons. First, they provide a warm-up case where one can check the lattice calculations in a simpler setting. The large discrete subgroup of the AdS isometries preserved by the tilings means that the full isometries are often "accidental" symmetries of the theory broken only by high dimension operators that scale away quickly at long distances. Second, if the initial maximally symmetric tiling has triangles that are not much larger than the spatial curvature, then the effect of the curvature within a single triangle is small and further refinements of the tiling are approximately those of flat space. Finally, most known physical systems have critical exponents that are $\mathcal{O}(1)$, which translates to their AdS duals having fields with masses m comparable to the AdS radius. Therefore their Compton wavelength is generally spread out over sizes similar to ℓ and perhaps even the tilings without refinement may give good approximations to boundary CFT observables.

This paper is organized as follows. In Sec. II, we review the triangle group that we use to construct maximally symmetric tilings of hyperbolic space, and set up the discretized action for a scalar field theory on this lattice. In Sec. III, we characterize the behavior of the classical theory on this lattice and compare to analytic results. Most of the discussion in Sec. III will focus on the free theory, where we compute various propagators and quantify how they differ on the lattice vs in the continuum, but we also compare lattice and continuum results for a tree-level four-point function in $\lambda\phi^4$ theory. In Secs. IV and V, we go beyond our maximally symmetric lattices and study how additional corrections can be included in order to approach the continuum limit; Sec. IV focuses on finite volume effects, and Sec. V shows how to refine the lattices to make the lattice spacing arbitrarily small in units of the radius of curvature of hyperbolic space. Finally, in Sec. VI we conclude with a discussion of future directions.

II. TILING THE HYPERBOLIC DISK

Euclidean de Sitter $\mathbb{S}^d$ and anti–de Sitter $\mathbb{H}^d$ space have constant positive and negative curvature, respectively. Although in the continuum they share with flat space $\mathbb{R}^d$ the attribute of being a maximally symmetric Riemann manifold, they pose new difficulties for lattice construction. A lattice realization necessitates a scheme used to tile the geometry it represents. In $\mathbb{R}^d$ a common lattice choice is hypercubic (square, cubic, etc.) with a growing discrete subgroup of the isometries: integer translation on each axis on the torus and hypercubic rotation by $\pi/2$. In $\mathbb{H}^d$ all sites are equivalent; there is no "origin." Thus we already see one additional challenge in tiling a space with constant negative curvature. In what follows, we detail how to tile AdS by constructing a simplicial lattice for hyperbolic space using the triangle group.

Although the goal of this section is to construct a simplicial lattice of $\mathbb{H}^2$, it is interesting to see this in the context of the three maximally symmetric manifolds of either positive, negative, or zero constant curvature. The full Euclidean plane $\mathbb{R}^2$ (adding a point at infinity) is equivalent to the Riemann sphere up to a Weyl factor:

$$ds^2_{\mathbb{R}^2} = dx^2 + dy^2 \to ds^2_{\mathbb{S}^2} = 4\ell^2 \frac{dz d\bar{z}}{(1+|z|^2)^2}, \qquad (2.1)$$

where the scalar curvature $K = 1/\ell^2$ and ℓ is the radius of the sphere. Similarly, hyperbolic space with $K = -1/\ell^2$ can be represented as the Euclidean upper half-plane (UHP) up to a Weyl factor $1/y^2$, which can then be mapped to the Poincaré disk

$$ds^2_{UHP} = \ell^2 \frac{dx^2 + dy^2}{y^2} \to ds^2_{\mathbb{H}^2} = 4\ell^2 \frac{dz d\bar{z}}{(1 - |z|^2)^2} \tag{2.2}$$

by the Möbius transformation $w = x + iy = -i(z + 1)/(z - 1)$ with $|z| < 1$. The Poincaré disk is most convenient for our triangulation. The $PSL(2, \mathbb{Z})$ isometries in the UHP are real Möbius transformations, $w \to w' = (aw + b)/(cw + b)$, which are easily mapped to Poincaré disk coordinates. This includes rotations that are manifest in polar coordinates on the Poincaré disk with $z = re^{i\theta}$. Unlike the sphere, the boundary at $r = 1$ is at geodesic infinity, which can be seen from the metric $ds^2 = d\rho^2 + \sinh^2(\rho) d\theta$ with the radial geodesic coordinate $\rho = \log[(1 + r)/(1 - r)]$. We will proceed to use the triangle group to tessellate the Poincaré disk with approximately concentric layers around $r = 0$.

A. The triangle group

If p, r, and q are integers greater than one, the full triangle group $\Delta(p, r, q)$ is a group that can be realized geometrically as a sequence of reflections along the sides of a triangle with angles $(\pi/p, \pi/r, \pi/q)$. The *proper* rotation triangle group, $D(p, r, q)$, is generated by two elements S, T satisfying $S^p = T^q = U^r = 1$, where $U = ST$. The target space is tessellated by acting on an initial triangle with angles $(2\pi/p, 2\pi/r, 2\pi/q)$ in each vertex. The full *improper* triangle group includes a $\mathbb{Z}_2$ factor for reflections a, b, c on the edges, with $a^2 = b^2 = c^2 = 1$. Two reflections along the sides joining at a vertex give a rotation around that vertex: $S = ab, T = bc, U = ca$. Either way the result is a uniform triangulation of a manifold with constant positive, zero or negative curvature dictated by the sum rule:

$$\frac{\pi}{p} + \frac{\pi}{r} + \frac{\pi}{q} \begin{cases} > \pi & \text{positive curvature} \\ = \pi & \text{zero curvature} \\ < \pi & \text{negative curvature} \end{cases} \tag{2.3}$$

The group is finite for positive curvature and infinite for flat and hyperbolic space [12].

As a familiar example start with flat space where $D(3, 3, 3)$ generates the triangular lattice. At a more fundamental level, we can start with the $D(2, 3, 6)$ group of 90-60-30 triangles and combine 6 of them together to create an equilateral triangle with 6 subtriangles. Dropping the midpoint recovers the $D(3, 3, 3)$ equilateral tessellation. In the same spirit $D(2, 4, 4)$ utilizes the right triangle for the standard square lattice and the hexagonal lattice is the dual of $D(3, 3, 3)$. We are most interested in the special series $D(2, 3, q)$, which divides equilateral hyperbolic triangles into 6 subtriangles, thereby generalizing the 90-60-30 degree flat case to a triangle with 90-60-$(30 \cdot \frac{6}{q})$ degree interior angles. An important feature of hyperbolic/spherical triangles is the introduction of an intrinsic length scale, $\ell^2 = \pm 1/K$ in terms of the scalar curvature K. This fixes the area of the hyperbolic and spherical triangles,

$$A_\Delta = |\pi - \alpha - \beta - \gamma| \ell^2, \tag{2.4}$$

in terms of the interior angles (α, β, γ) and the intrinsic scale ℓ. Whereas in flat space the scaling gives no condition on the area, in the spherical case there is a maximum triangle area of $2\pi\ell^2$ given by a great circle. Perhaps a bit surprisingly, in hyperbolic space there is also a maximum area of $\pi\ell^2$ when all interior angles vanish.

For positive curvature, $q = 3, 4, 5$ produces the finite group symmetries and tessellations of the `tetrahedron`, `octahedron` and `icosahedron`, respectively. The `cube` and the `dodecahedron` are the respective dual polyhedra of the octahedron and icosahedron, thus completing the five Platonic solids.

The situation for $\mathbb{H}^2$ is more interesting. Even restricting ourselves to equilateral triangle graphs, starting with the infinite sequence $D(2, 3, q)$ for any $q \geq 7$ gives an infinite discrete subgroup[2] of hyperbolic isometries $PSL(2, \mathbb{R})$. The smallest triangles with the smallest curvature defect at the vertices is given by $q = 7$ and will be the major focus of our lattice construction.

B. Constructing the lattice

From the above discussion, the hyperbolic plane can be tiled with $\Delta(2, 3, q)$ where q is any integer with $q \geq 7$. One of the benefits of a lattice built up from $\Delta(2, 3, q)$ is that there is a $\mathbb{Z}_q$ symmetry. This can be exploited to simplify calculations and also provides a check for the structure we expect in certain data. The case $q = 7$ is particularly nice as it gives triangles in AdS_2 with the smallest area and therefore the least curvature (cf. Appendix A 2 for details). We mention in passing that the case $q = 8$ is also useful in that a geodesic connecting two points will always pass through lattice points.

In practice the lattice is constructed as follows:

[2]These groups have fascinating properties studied exhaustively in the mathematics literature [13–15]. The full modular group, $PSL(2, \mathbb{Z})$, is reached in the limit $q \to \infty$. In special cases they yield finite representations of constant negative curvature Riemann surfaces—the negative curvature analogue of Platonic solids. A famous example is the 168 element tessellation of the genus 3 surface, first introduced by Felix Klein in 1879, (reprinted in [13]), in the study of the Riemann surface associated with the "Klein quartic", $x^3y + y^3z + z^3x = 0$. For a historical account of this work, see [13–16].

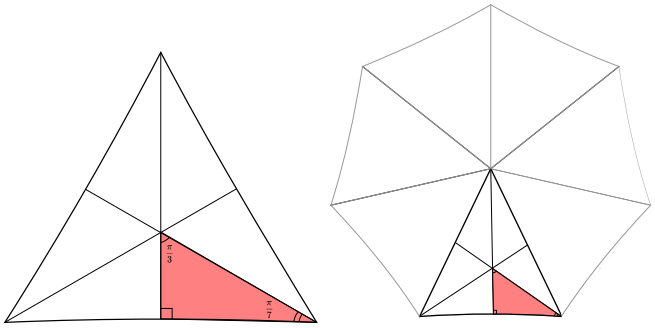

FIG. 1. We construct the lattice using hyperbolic equilateral triangles built from the $\Delta(2,3,q)$ triangle group. Left: the hyperbolic equilateral triangle $(2\pi/7, 2\pi/7, 2\pi/7)$ built from the $\Delta(2,3,7)$ triangle group. Right: the first layer of the lattice constructed by rotating the $(2\pi/7, 2\pi/7, 2\pi/7)$ equilateral triangle around a point.

(i) Choose q, which sets the properties of the equilateral triangle such as its area and side length.
(ii) Put the first lattice point at the origin ($r = 0$) of the Poincarè disk. Put the second on the real axis a distance of the side length of the equilateral triangle.
(iii) Rotate by $2\pi/q$ around the origin to add additional triangles until the layer is complete.
(iv) Move out to a point on the next layer. Rotate around this point by $2\pi/q$ but laying triangles only along forward links connecting to the following layer.
(v) Continue until the input layer L is reached.

Figure 1 illustrates the construction of a hyperbolic equilateral triangle built from the triangle group with $q = 7$. Figure 2 shows a $L = 4$, $q = 7$ tiling on the Poincarè disk and its dual realized from this construction. It is also possible to generate the lattice using the action of the triangle group on the lattice (cf. Appendix B). For generating large lattices using C-code we use the first method; for smaller lattices to which we will later add refinements, we use *Mathematica* utilizing the second method. Finally, we note that lattices can also be generated starting with the circumcenter of the equilateral triangle at the center ($r = 0$). However with a finite number of layers, this choice preserves for any q only an exact 3-fold rotational symmetry, rather than preserving a q-fold symmetry.

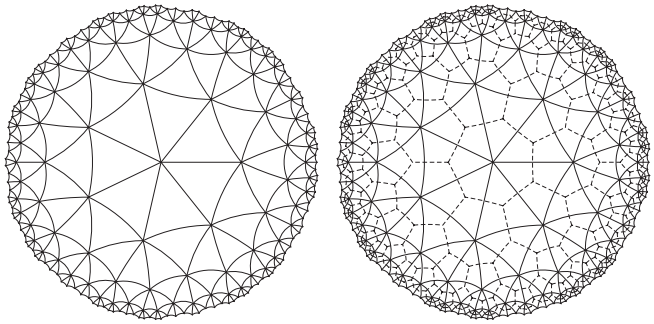

FIG. 2. Left: the $L = 4$, $q = 7$ lattice on the Poincaré disk. Right: the same lattice with the dual lattice shown in dotted lines. In the infinite L limit we produce a tiling of the entire Poincaré disk.

C. Lattice action for scalar fields

We choose ϕ^4 theory as a simple example with the action

$$S = \frac{1}{2}\int d^2x\sqrt{g}(g^{\mu\nu}\partial_\mu\phi\partial_\nu\phi + m^2\phi^2 + \lambda\phi^4). \tag{2.5}$$

Discretizing this action on a 2d triangulated lattice (or indeed any d-dimensional simplicial complex) takes the generic form,

$$S = \frac{1}{2}\sum_{\langle ij\rangle} K_{ij}(\phi_i - \phi_j)^2 + \frac{1}{2}\sum_i \sqrt{g_i}(m^2\phi_i^2 + \lambda\phi_i^4), \tag{2.6}$$

where the sum is over the sites i and the links $\langle ij\rangle$ on the graph. The coefficients $\sqrt{g_i}$ and K_{ij} can be determined by the finite element method literature (FEM) [17] as presented in detail for positive curvature triangulation in Refs. [18,19]. This method sets the measure $\sqrt{g_i}$ to the volume at dual sites (e.g., the heptagons in Fig. 2) and the kinetic weights K_{ij} to the ratio S_{ij}/l_{ij} of the dual to the link (the Hodge star of the link l^*_{ij}) divided by length of the link l_{ij}. In fact, these kinetic weights K_{ij} were anticipated in the pioneering paper by N. Christ, R. Frieberg and T.D. Lee [20] by enforcing a discrete Gauss' law constraint on a random lattice and later generalized as a consequence of discrete exterior calculus (DEC) [21] on a simplicial complex.

For our $\Delta(2,3,q)$ example, illustrated in Fig. 3 for $q = 7$, the tessellation consists of uniform equilateral triangles so that both $\sqrt{g_i}$ and K_{ij} are constants independent of position. On the hyperbolic disk they are given as

$$\sqrt{g_i} = \frac{q}{3}A_\Delta, \qquad K_{ij} = \frac{4A_\Delta}{3a^2}, \tag{2.7}$$

in terms of the area $A_\Delta = (\pi - 6\pi/q)\ell^2$ of the equilateral triangle and the lattice spacing a, which is the length of each side of the triangle, defined below in (2.10). In our numerical work we have adopted the common practice of setting $K_{ij} = 1$ by an appropriate re-scaling of the field ϕ. We also have introduced a dimensionless bare mass parameter,

$$m_0^2 \equiv c_q^2 m^2, \qquad c_q^2 = \frac{\sqrt{g_i}}{K_{ij}} = \frac{qa^2}{4}, \tag{2.8}$$

in terms of an effective lattice spacing $c_q = q^{1/2}a/2$, as well as a re-scaled coupling $\lambda_0 = 3qa^4\lambda/(16A_\Delta)$. Now in our simulations in the triangle group lattice, the action takes the convenient form

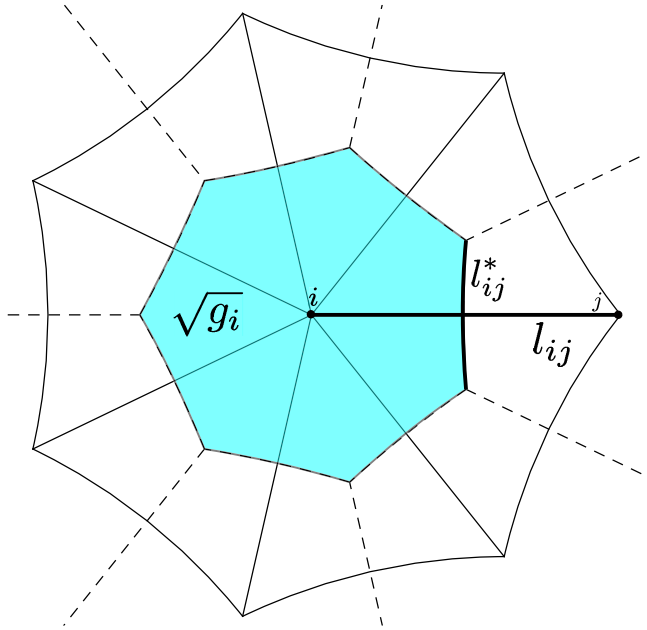

FIG. 3. The lattice and its dual at a vertex point i. The area of the dual heptagon (light blue region) corresponds to $\sqrt{g_i}$ and the kinetic weight between i and another point j is given by $K_{ij} = l_{ij}/l^*_{ij}$.

$$S = \frac{1}{2}\sum_{\langle ij\rangle}(\phi_i - \phi_j)^2 + \frac{1}{2}\sum_i (m_0^2\phi_i^2 + \lambda_0\phi_i^4). \tag{2.9}$$

Restoring the dimensionful form is easily done when we compare the simulation to the continuum.

All lattice calculations in flat space have to deal with both lattice spacing (UV) and finite volume (IR) errors. In flat space, on a toroidal hypercubic lattice, the lattice spacing a for a finite volume $V = (aL)^d$ has a single integer ratio $L = V^{1/d}/a$, which is the number of lattice spacings in a closed cycle. Since flat space has no intrinsic scale the lattice spacing is arbitrary and only defined relative to some physical mass scale $m^{-1} = a\xi$. Control over UV and IR errors requires a window such that $a \ll m^{-1} \ll aL$.

Hyperbolic space (or de Sitter space) is different because the manifold itself has an intrinsic length scale given by the curvature. Thus even the infinite lattice has two scales, the UV cut-off and the curvature, which complicates the problem of approximating a continuously smooth manifold of constant negative curvature with objects of a finite size. Additionally, there is no analogue to periodic boundary conditions to *hide* the finite volume boundary. Instead, the boundary is an important feature exploited by AdS/CFT, which we discuss later.

The intrinsic continuum scale ℓ of the manifold is provided by the metric (A1). The area of a hyperbolic (or spherical) triangle A_Δ is determined by the deficit angle $|\pi - \alpha - \beta - \gamma|$. In units of ℓ^2 the area is bounded by $A_\Delta/\ell^2 < \pi$. For our $(2, 3, q)$ equilateral triangulation of the disk the length of the edges a is given by

$$\cosh(a/2\ell) = \frac{\cos(\pi/3)}{\sin(\pi/q)} = \frac{1}{2\sin(\pi/q)}, \tag{2.10}$$

which gives the minimum values of $a = 1.090550\ell$ and $A_\Delta = 0.448799\ell^2$ for $q = 7$. Note that as $q \to \infty$ the length diverges logarithmically as $a \cong 2\ell\log(q)$ but the area approaches the so-called ideal hyperbolic triangle area of $A_\Delta = \pi\ell^2$. We focus exclusively on the case $q = 7$ that gives the minimum intrinsic lattice scale.

D. Lattice simulations

Our lattice simulation generates a graph by starting with a vertex at $r = 0$ and building out one layer of triangles at a time to L layers. Each layer has $n[L]$ vertices, where $n[L]$ satisfies the recursion relation (cf. Appendix C)

$$\begin{aligned} n[L] &= (q-4)n[L-1] - n[L-2], \\ n[1] &= q, \qquad n[0] = 0. \end{aligned} \tag{2.11}$$

In this graph the growth of vertices is exponential in L. Additionally, at asymptotically large L the last layer has a finite fraction of all the points in our lattice. For $q = 7$ this fraction is the inverse of the Golden Ratio, $2/(1+\sqrt{5}) \approx 61\%$ of all points. For a finite number of layers, our lattice has only a finite volume and fills out the Poincaré disk with a cut-off, i.e., $|z| \le 1 - \epsilon$. We place fields ϕ_i on the interior vertices, labeled by r_i, θ_i, and impose Dirichlet boundary conditions on a fictitious $(L+1)$th layer. Not all points on this layer are at the same distance from the "origin," since our lattice breaks rotational invariance to a discrete subgroup. Nevertheless, we can define an approximate cutoff in $1 - |z|$ by taking its value averaged over all points on this fictitious layer, where the boundary condition is enforced:

$$\epsilon_{\text{eff},L} = \text{mean}_{i\in(L+1)\text{th layer}}(1 - |z_i|) \propto e^{-0.919\ell(L+1)}. \tag{2.12}$$

This IR cutoff $\epsilon_{\text{eff},L} \propto e^{-\tilde{c}_7\ell(L+1)}$ can be thought of as an effective lattice length $\tilde{c}_7 = 0.919$ in the radial direction. This numerical estimate, extrapolating from finite L, is very close to the asymptotic lattice spacing, $a_7 = 0.962$, between layers in (C10). Also note that $\tilde{c}_7$ is approximately two-thirds of the UV scale $c_7 = \sqrt{q/4}(a/\ell) = 1.443$ that we introduced above.

III. CLASSICAL THEORY ON TRIANGLE GROUP LATTICE

In this section we mostly study the free discretized theory in AdS_2, the action (2.6) with $\lambda = 0$, with a focus on the errors introduced by the UV cut-off and IR finite volume effects. The continuum limit in the free theory is of

course solvable and will allow us to check our methods and analyze discretization errors, and will give insight into features that are absent in the flat space formulation. Moreover, the main quantities of interest in the free theory are propagators, which we will use in later sections to do perturbative computations at weak coupling.

A. Green's function

We begin by considering the bulk-to-bulk propagator in AdS. Both the bulk-to-boundary propagator and the boundary-to-boundary two-point function in the dual CFT can be extracted from the bulk Green's function, so in this sense it is a more basic building block than the others. There is another practical reason, however, for beginning with the bulk propagator, namely our finite lattices can never truly reach infinity and consequently we will have to be more careful than usual when extracting propagators with points on the boundary.

We begin with a brief review of some well-known results in the continuum limit. For a given mass-squared m^2, the analytic bulk Green's function $G_{bb}(X, X')$ between two points X, X' in AdS_{d+1} is the solution to the equation

$$(-\nabla^2 + m^2)G = \frac{1}{\sqrt{g}}\delta^{d+1}(X - X'), \tag{3.1}$$

where ∇_μ is the covariant derivative $\frac{1}{\sqrt{g}}\delta^{d+1}(X - X')$ defined as the δ function for AdS_{d+1}, and the Laplace operator is $\nabla^2 = \nabla_\mu \nabla^\mu = \sqrt{g}^{-1}\partial_\mu \sqrt{g} g^{\mu\nu}\partial_\nu$ acting on scalars. The solution is given by [22,23]

$$\begin{aligned} G_{bb}(X, X') &= G_{bb}(\sigma(X, X')) \\ &= e^{-\Delta\sigma(X,X')}{}_2F_1\left(\Delta, \frac{d}{2}, \Delta + 1 - \frac{d}{2}; e^{-2\sigma(X,X')}\right), \end{aligned} \tag{3.2}$$

where $m^2\ell^2 = \Delta(\Delta - d)$ and $\sigma(X, X')$ is the geodesic distance between the points X and X'. For $d=1$ and $\Delta=1$ this reduces to the simple value of

$$G_{bb}(\sigma) \overset{\Delta=1}{=} \frac{1}{2}\log\coth\frac{\sigma}{2}. \tag{3.3}$$

For the geodesic distance σ in various coordinate systems, see Appendix A 1.

For the most part, we will not need the exact form of the propagator because the lattice spacing is comparable to the AdS radius and distinct lattice points have a minimum geodesic distance between them. Above, we saw that this geodesic distance is smallest for $q = 7$ where it is $\sigma_{\min} = a = 1.09\ell$, and so $e^{-2\sigma} \leq 0.11$ for our lattice points. We can therefore approximate the hypergeometric function ${}_2F_1(\Delta, \frac{1}{2}, \Delta + 1 - \frac{1}{2}; t^2)$ in the propagator as ≈ 1. In fact, between $\Delta = 1$ and $\Delta = \infty$, this propagator interpolates between the simple functions $\frac{1}{t}\tanh^{-1} t$ and $(1 - t^2)^{-\frac{1}{2}}$, and these never deviate from 1 by more than ~ 6 percent over the range $0 < t^2 < 0.11$. Consequently, we will often approximate the propagator as simply

$$G_{bb}(\sigma) \approx e^{-\Delta\sigma}. \tag{3.4}$$

Both the finite lattice spacing as well as the finite number of layers make the exact bulk Green's function more complicated in the discretized theory than in the continuum limit, and we will not be able to write it down in closed form. However, in the following we will be able to obtain closed form approximations in various limits.

B. Taylor expansion of lattice action

The discretized bulk Green's function is simply the inverse G_{ij} of the matrix A_{ij} from the free theory action,

$$\begin{aligned} S &= \frac{1}{2}\phi_i A_{ij}\phi_j = \frac{1}{2}\left[\sum_{\langle ij\rangle}(\phi_i - \phi_j)^2 + \sum_i m_0^2\phi_i^2\right] \\ &= \frac{1}{2}\sum_i\left[\frac{1}{2}\sum_{j \text{ adjacent to } i}(\phi_i - \phi_j)^2 + m_0^2\phi_i^2\right]. \end{aligned} \tag{3.5}$$

The sum on $\langle ij\rangle$ is over adjacent pairs of points. Because each lattice point has q neighbors, the matrix A_{ij} is $q + m_0^2$ on the diagonal, -1 in off-diagonal entries if i and j are neighboring points, and 0 otherwise.

We would like to relate the discretized action to the continuum action. To do this, we can Taylor expand ϕ around each point to leading order in the lattice spacing:

$$\phi_j - \phi_i \approx r_j^\mu \cdot \nabla_\mu\phi(r_i). \tag{3.6}$$

The Taylor expansion uses the covariant derivative ∇_μ to account for the curvature of space, and the magnitude of $\vec{r}_j$ should be the geodesic length between i and j. Because there is a $\mathbb{Z}_q$ subgroup of the rotational symmetry around each point, all such adjacent distances are the same lattice spacing a. Moreover, it is easy to see that

$$\sum_{j \text{ adjacent to } i} r_j^m r_j^n = \frac{qa^2}{2}\delta^{mn}. \tag{3.7}$$

The fact that the right-hand side (rhs) must be proportional to δ^{mn} is due to the $\mathbb{Z}_q$ symmetry, and the proportionality constant can be obtained by taking the trace of both sides of the equation. Therefore, at leading order in a, the discretized free action is equivalent to the following continuum action

$$S \approx \frac{3a^2}{4A_\Delta}\int d^2x\sqrt{g}\left[\frac{1}{2}(\nabla\phi)^2 + \frac{1}{2}m^2\phi^2\right], \tag{3.8}$$

where we re-instated the original mass parameter m^2 using (2.7).

If the lattice spacing a could be taken arbitrarily small, then we could simply expand the discretized kinetic term to leading order in a. In our case, the lattice spacing a is fixed by our choice of triangle group and has a minimum possible value in units of the AdS radius ℓ, so cannot be taken arbitrarily small. Therefore, to improve the accuracy of the approximation, we may need to keep higher order terms in the Taylor expansion. The result for $q = 7$ is that due to the $\mathbb{Z}_7$ symmetry, the action expanded to $\mathcal{O}(a^{12})$ can be written in terms of powers of the rotationally symmetric combination ∇^2:

$$S \propto \int d^2x\sqrt{g}\left[\frac{1}{2}(ma)^2\phi^2 - \frac{1}{2}\phi\left(\sum_{s=1}^{6} b_s(a^2\nabla^2)^s + \mathcal{O}(a^{14})\right)\phi\right], \tag{3.9}$$

where we have found the coefficients b_s to be

$$b_1 = 1, \qquad b_2 = \frac{1}{16}, \qquad b_3 = \frac{1}{576},$$
$$b_4 = -\frac{7}{36,864}, \qquad b_5 = -\frac{7}{30,700},$$
$$b_6 = -\frac{77}{88,473,600}. \tag{3.10}$$

Starting at $\mathcal{O}(a^{14})$ and higher, one finds combinations of derivatives that break rotational invariance but preserve the $\mathbb{Z}_7$.

Now, we can obtain an approximate formula for the discretized bulk-to-bulk propagator $G_{\mathrm{bb,lat}}$ that is valid at small m^2. To do this, recall that (for $\sigma > 0$) the continuum bulk-to-bulk propagator G_{bb} satisfies

$$\nabla^2 G_{bb} = \frac{1}{\ell^2}\Delta(\Delta - 1)G_{bb}. \tag{3.11}$$

If we take G_{bb} with Δ a free parameter and substitute it into the equation of motion for our series expanded action (3.9), we find that it is a solution as long as

$$m^2a^2 = \sum_{s=1}^{6} b_s\left(\frac{a^2}{\ell^2}\Delta(\Delta - 1)\right)^s. \tag{3.12}$$

Note that $\Delta = 1$ remains a solution at $m^2 = 0$. By continuity, as long as m^2 is sufficiently small Δ will be close to 1, and discarding the $\mathcal{O}(a^{14})$ terms and higher will be a good approximation. In Fig. 4, we compare the prediction of the analytic equation (3.12) with fits to the numerical data, at small mass. The figure also shows the prediction of another analytic equation valid at large mass, which we derive in the next subsection.

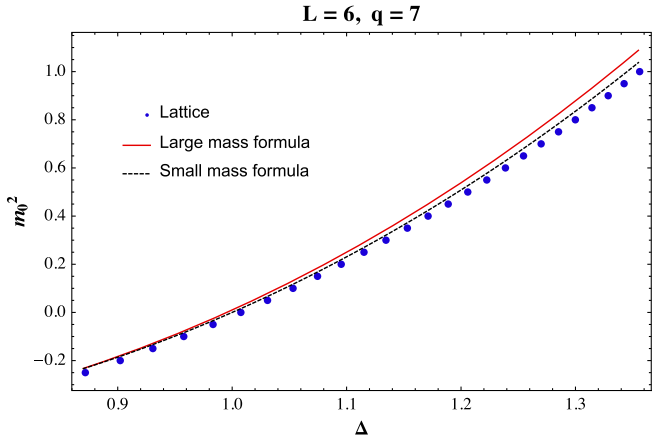

FIG. 4. A comparison of the mass-squared scaling dimension from the lattice data to the expansion formula (3.12) and the asymptotic analysis formula (3.19) for small masses. Dots are extracted from lattice data as described in subsection III D.

C. Large mass effective model

The approximation in the previous subsection for the bulk-to-bulk propagator breaks down when m^2 is too large. Here, we will consider a different approximation that works well for large m^2.

Consider the equation of motion for G_{ij} as a function of j with i fixed, in the limit of large geodesic separation σ. With an infinite number of layers, we can take any point i to be the center of our triangulated lattice without loss of generality. Additionally, near the boundary of AdS there is a lattice point at every θ (see Fig. 2), but by contrast the lattice spacing in ρ remains the same regardless of the layer. We can use this fact to obtain an approximate formula for the discretized Green's function G_{ij} at large σ by letting G be independent of θ, due to rotational symmetry, and letting ρ be discrete in the free AdS equation of motion.

In the continuum the metric can be written (see A 1) as $ds^2 = d\rho^2 + \sinh^2(\rho)d\theta$. Assuming rotational symmetry the equation of motion is

$$-\partial_\rho^2 G(\rho) - \coth(\rho)\partial_\rho G(\rho) + m^2 G(\rho) = \partial_\rho\delta(\rho), \tag{3.13}$$

where ρ is the radial geodesic distance from the source at the origin.

At large ρ the Green's function therefore satisfies the equation,

$$-\partial_\rho^2 G(\rho) - \partial_\rho G(\rho) + m^2 G(\rho) \cong 0. \tag{3.14}$$

Different ways of discretizing the ∂_ρ derivatives lead to different solutions for $G(\rho)$. To see this, let us factor out an overall exponential dependence from $G(\rho)$:

$$G(\rho) = e^{s\rho}g(\rho). \tag{3.15}$$

The equation of motion in terms of $g(\rho)$ is

$$s(1+s)g(\rho)+(1+2s)g'(\rho)+g''(\rho)=m^2\ell^2 g(\rho). \quad (3.16)$$

The left-hand side (lhs) of (3.16) can be discretized by the following finite difference:

$$\text{LHS} \approx \frac{(2bs+b+2)g(\rho+b)}{2b^2} + \left(s^2+s-\frac{2}{b^2}\right)g(\rho) - \frac{(2bs+b-2)g(\rho-b)}{2b^2}. \quad (3.17)$$

The resulting finite difference equation, like the continuum equation, has a growing and decaying solution at $\rho\to\infty$. The decaying solution behaves at large ρ as $G(\rho)\sim e^{-\Delta\rho}$ for some Δ. Substituting $g(\rho)=e^{-(\Delta+s)\rho}$ into our discretized equation of motion, we see that the equation is satisfied as long as Δ obeys the following equation:

$$2(\cosh(b(\Delta+s))-1)-b(2s+1)\sinh(b(\Delta+s)) = b^2(m^2\ell^2-s(s+1)). \quad (3.18)$$

At large m^2, the solution is $\Delta+s\sim b^{-1}(\log m^2\ell^2+\log(\frac{b^2}{1-b(s+\frac{1}{2})}))$, whereas in the limit $b\to 0$ of small lattice spacing, the solution reduces to the usual $m^2\ell^2=\Delta(\Delta-1)$. The parameters s and b are fudge factors that we use to compensate for the fact that our finite difference equation treats the lattice like a set of regularly spaced points in ρ, whereas the true lattice equation involves differences in multiple different directions and is more complicated. We have found that the choice $s=-1/2$, i.e.,

$$m^2\ell^2=\left(\frac{4}{b^2}\sinh^2\left(b\frac{\Delta-\frac{1}{2}}{2}\right)-\frac{1}{4}\right), \qquad b=\begin{cases}0.96 & 7\\ 1.34 & 8\\ 1.66 & 9\end{cases} \quad (3.19)$$

approximates the exact numeric results quite well with the given values of b for $q=7$, 8, 9, as shown in Fig 5, where we compare at large masses the analytic approximation (3.19) with the numeric values of Δ extracted from the data; in Fig 5, we also show for comparison the prediction of the small mass analytic expression (3.19) from the previous subsection. Note that $s=-1/2$ is special in that it respects the $\Delta\to 1-\Delta$ symmetry of the m^2 vs Δ relation of the continuum theory. Also note that in Appendix C we determine analytically the mean lattice spacings between layers to be $a_q=0.9624$, 1.317, 1.567 for $q=7$, 8, 9, which are nearly identical to the values of b found here by fitting to the correlator data.

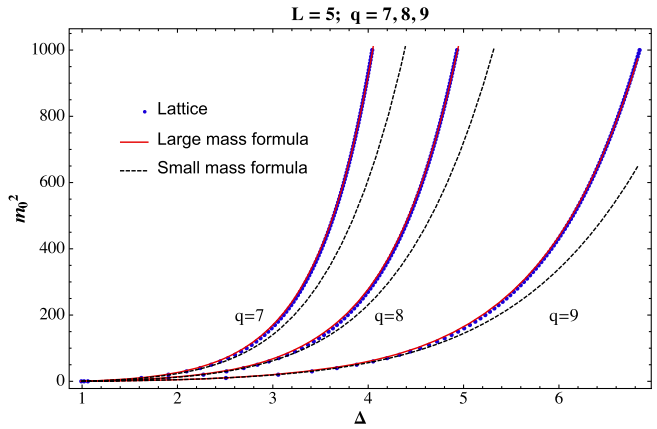

FIG. 5. Same as Fig. 5 but for large masses. Dots are extracted from lattice data, black dashed and red solid curves are the expansion formula (3.12) and the asymptotic analysis formula (3.19) respectively.

D. Numerical propagator and comparison

Once we have the lattice action in the form (3.5), the numeric computation of the bulk Green's function G_{ij} just requires taking the inverse of A_{ij}. In this subsection, we will inspect the numeric Green's function and see how it compares to the analytic results derived above.

Recall the approximate formula for the continuum bulk-to-bulk propagator:

$$\log G_{bb}(\sigma)\approx -\Delta\sigma. \quad (3.20)$$

From the previous subsections, we expect that the discretized bulk-to-bulk propagator will behave similarly, but with a modified value for Δ compared to the usual continuum limit relation $m^2\ell^2=\Delta(\Delta-1)$. Our strategy will therefore be to first check that $\log G$ is approximately linear in σ, and then from its slope extract Δ. By doing this for many values of m^2, we obtain the function $\Delta(m^2)$. Typical plots of $\log G$ as a function of σ for fixed m^2 are given in Fig. 6. These show that for the lattice propagator, $\log G_{bb}(\sigma)$ is indeed linear in σ.

Figure 6 also shows how only using bulk points in the linear fit to avoid boundary effects we can improve the derived Δ. Additionally, in Sec. V we show how using the exact fit from taking into account the true finite boundary condition produces a remarkably good estimate for Δ for a modestly size lattice. However, the approximate linear fit is sufficient for most of our purposes, as noted before.

The result of this comparison of the lattice propagator to our small and large mass approximate formulas [(3.12) and (3.19), respectively] is shown in Figs. 4 and 5, showing an excellent agreement over a large range in mass.

1. Approach to cutoff boundary

One subtlety in our tessellation scheme that we need to account for is that the lattice boundary points, although

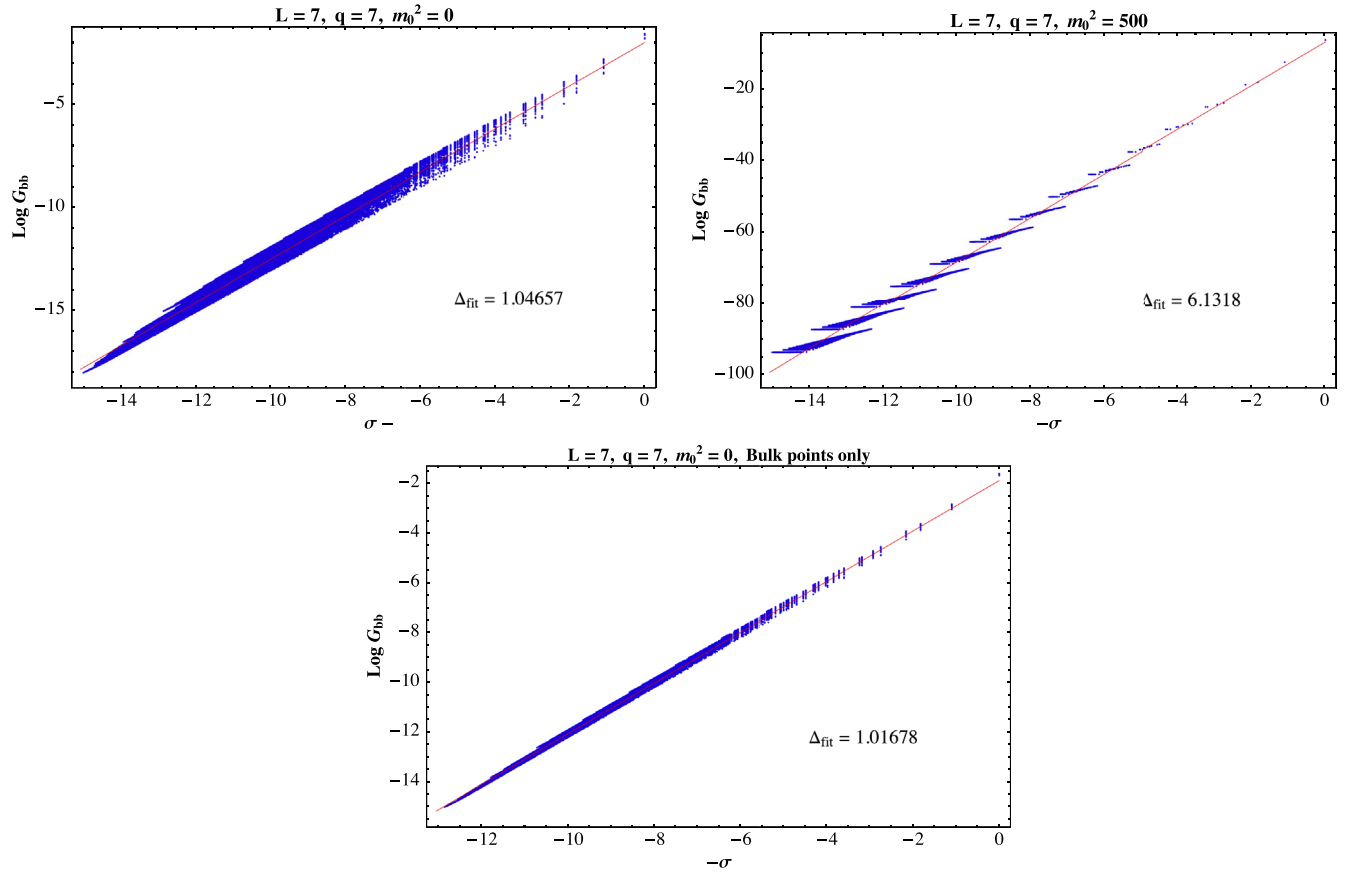

FIG. 6. A plot of (3.20) for different mass regimes. In the top plots the source point X and sink point X' cover all possible pairs on the lattice from which Δ_{fit} is derived from. In the bottom plot, only bulk points are used to avoid boundary effects. The linear fit is evident.

close, are not all at the same distance away from the origin on the Poincaré disk. This will affect comparing boundary dependent observables, such as the bulk-to-boundary propagator. We can see this by looking at the bulk-to-boundary propagator as the limit of the bulk-to-bulk propagator as the primed bulk coordinate approaches the boundary via $y' \to 0$:

$$G_{b\partial}(y, x, x'; \Delta) = \left(\frac{y}{y^2 + |x - x'|^2}\right)^{\Delta} = \lim_{y' \to 0} \frac{1}{y'^{\Delta}} G_{bb}(y, x, y', x'; \Delta), \quad (3.21)$$

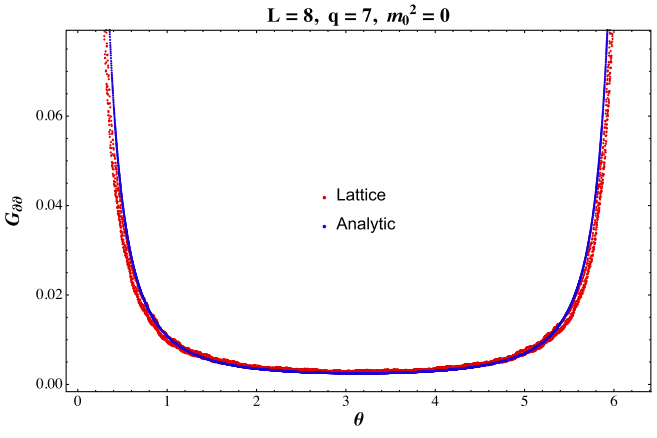

FIG. 7. Boundary-boundary two-point function from one point fixed on the boundary to all others, for lattice vs analytic continuum result.

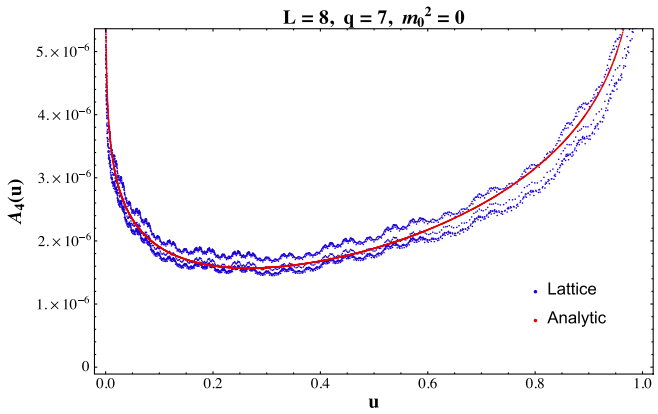

FIG. 8. Four-point contact term from lattice vs analytic continuum result (3.27).

where as $y' \to 0$ the divergent part goes as

$$(y')^{-\Delta} \sim (1 - |z'|^2)^{-\Delta}. \tag{3.22}$$

So when looking at the bulk-to-boundary propagator from one point on the boundary, X, to any other point X', we need

$$G_{b\partial}(X, X'; \Delta) \simeq (1 - |z'|^2)^{-\Delta} G_{bb,\mathrm{lat}}(X, X'; \Delta), \tag{3.23}$$

where $G_{bb,\mathrm{lat}}$ indicates the numeric lattice propagator data. In Fig. 7, we compare the result from the lattice data to the exact CFT two-point function, which in our θ coordinate is

$$G_{\partial\partial}(\theta) \propto (1 - \cos\theta)^{-\Delta}, \tag{3.24}$$

where the proportionality constant depends on the normalization of the operator, which we fix to match the lattice data.

E. Four-point function

Now that we have characterized the propagators we can calculate tree diagrams. Here we focus on the four-point interaction term, which has a known analytic form. The AdS_2 four-point contact term is given by

$$A_4^{\mathrm{Contact}}(x_i) = D_{\Delta_1\Delta_2\Delta_3\Delta_4} = \int d^2y \sqrt{g(y)} G_{b\partial}(y, x_1) G_{b\partial}(y, x_2) G_{b\partial}(y, x_3) G_{b\partial}(y, x_4). \tag{3.25}$$

This becomes a sum on the lattice

$$A_4^{\mathrm{Contact}}(x_i) \to \sum_i a_i^{\Delta} G_{b\partial}(x_i, x_1) G_{b\partial}(x_i, x_2) G_{b\partial}(x_i, x_3) G_{b\partial}(x_i, x_4), \tag{3.26}$$

where a_i^{Δ} is the area of the lattice triangle being summed over. Therefore we can easily calculate the four-point function by summing over four bulk-to-boundary propagator configurations. Moreover, for $\Delta_1 = \cdots = \Delta_4 = 1$ the D-function has a closed form given by

$$\frac{2x_{13}^2 x_{24}^2}{\pi^{d/2}} D_{1111}(x_i) = \frac{1}{z - \bar{z}} \left(2Li_2(z) - 2Li_2(\bar{z}) + \log(z\bar{z}) \log\frac{1 - z}{1 - \bar{z}} \right), \tag{3.27}$$

which for $d = 1$, $z = \bar{z}$, and to leading order becomes

$$D_{1111}(x_i) \simeq \frac{2x_{13}^2 x_{24}^2}{\sqrt{\pi}} \left(-2\frac{\log(1 - z)}{z} + 2\frac{\log z}{z - 1} \right), \tag{3.28}$$

allowing us to compare with the lattice value. The result of this comparison is shown in Fig. 8, where we find a good agreement between the lattice and the analytic expression.

IV. FINITE VOLUME CORRECTIONS

In this section, we will discuss corrections to our discretization arising from the fact that any finite lattice fills out only a finite volume of AdS_2. We will approach these corrections in two different ways. The first is to compare our lattice results for the eigenvalues of the discretized Laplacian operator to the eigenvalues of a modified AdS_2 space where we move the boundary to a finite radius. The second is to consider modifying our discretized action to take into account the effect of "integrating out" the rest of the space not included in our finite volume region.

A. Eigenvalues of the Laplacian on finite disk

One measure of the accuracy of the lattice approximation is how closely the eigenvalues of the Laplacian are to the those of the continuum theory. AdS_2 has infinite volume and the eigenvalues of its Laplacian form a continuous distribution. However, for any finite number of layers, our tessellation fills out a finite volume, so it is more instructive

to compare the eigenvalues of our discrete system to those of AdS_2 with a finite cutoff at $r = 1 - \epsilon$ away from the original boundary at $r = 1$.

To find the spectrum of the Laplacian, we first solve the equation of motion locally. In global coordinates, take $f(r,\theta) = e^{il\theta} f(r)$ with integer l. The equation to solve is

$$\nabla^2 f(r,\theta) = -\lambda f(r,\theta) \to \frac{(r^2-1)^2(r(rf''(r)+f'(r)) - l^2 f(r))}{4r^2} = -\lambda f(r). \tag{4.1}$$

Next, we impose the boundary condition that the solutions are regular at $r = 0$. The regular solution is

$$f(r) \propto r^l (1-r^2)^{\frac{1}{2}+is}\, {}_2F_1\left(\frac{1}{2}+is, l+\frac{1}{2}+is; l+1; r^2\right), \tag{4.2}$$

where $s \equiv \sqrt{\lambda - \frac{1}{4}}$; although it is not obvious by inspection, the above function is invariant under $s \to -s$. The final step is to impose the boundary condition $f(1-\epsilon) = 0$. This condition can be imposed numerically, and for any $\epsilon > 0$ it is satisfied by the above solutions for a discrete set of values of λ. At $r = 1 - e^{-y}$ in the limit of large y (r close to 1) and small s, the eigenfunctions (4.2) are approximately proportional to $\sin(sy)$:

$$f(1-e^{-y}) \sim \frac{e^{-y/2}}{\pi^{1/2}\Gamma(l+\frac{1}{2})}\left[\frac{\sin sy}{s} + \left(\log(2) - \gamma_E - \psi\left(l+\frac{1}{2}\right)\right)\cos(sy) + \mathcal{O}(s)\right], \tag{4.3}$$

where $\psi(z)$ is the polygamma function and γ_E is the Euler-Mascheroni constant. Therefore, with a boundary at very large $y = \log\frac{1}{\epsilon}$ the eigenvalues are approximately given by the discrete spectrum

$$s = \frac{n\pi}{y}\left(1 + \frac{\gamma_E + \psi(l+\frac{1}{2}) - \log(2)}{y} + \mathcal{O}(y^{-2})\right), \quad n = 0, 1, 2, \ldots. \tag{4.4}$$

Since it is easy to numerically compute the exact spectrum of s for any boundary value ϵ using the exact eigenfunction (4.2), this is what we will use to compare to the lattice spectrum.

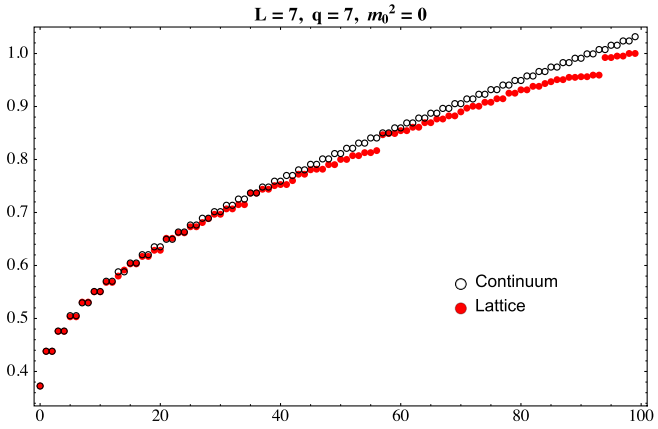

FIG. 9. The low-lying eigenspectrum of the continuum theory with a cutoff versus the discretized lattice realization. The normalization is fixed by matching the lowest eigenvalues, which is determined to lowest order by c_q^2. The slope is set by matching the second lowest eigenvalues. This can also be considered the definition of the cutoff.

For the massless $L = 7$, $q = 7$ lattice the mean cutoff can be estimated as $\epsilon_{\text{eff},7} \simeq 0.00082916$ by looking at the average value of $1 - r$ of the *next* $L = 8$ layer where the Dirichlet BC is enforced. However, by looking at the spectrum we can do even better in defining a cutoff. In comparing the lattice and continuum eigenspectrums there are two parameters we can fix, the offset and the slope. The offset is fixed by the normalization between the lowest eigenvalues, which is 2.013 in this case. We expect this to be close to the value given from the discrete Laplacian expansion at lowest order, $(7/4)(a^2/l^2) \simeq 2.081$. The slope is fixed by matching the second lowest eigenvalues. The result can be thought of as an improved definition for the cutoff, which in this case is $\epsilon_{\text{eff},7} \simeq 0.00080897$.

Figure 9 shows a comparison of the lattice spectrum versus the spectrum from the continuum theory with the improved ϵ cutoff. The first 100 out of 4264 eigenvalues plotted show the low-lying spectrum; there is a remarkable agreement between the lowest eigenvalues of the continuum theory and the unrefined lattice.

B. Integrating out the boundary

We can think of our lattice construction at finite L as a low-energy effective theory realized from starting with the

$L \to \infty$ limit and integrating out layers. Although the long-distance limit is associated with the IR, the modes of the dual CFT that live near the boundary are high energy ones, thus the Wilsonian intuition of "integrating out" is still valid. This is an example of the UV/IR connection. By integrating out layers, we can gain another quantitative handle on how observable quantities depend on the number of layers of the lattice, especially in the large L limit.

For a given L the lattice Hamiltonian has the structure

$$H = \left(\begin{array}{c|c} H_b & v \\ \hline v^T & H_\partial \end{array}\right), \tag{4.5}$$

where H_b contain the bulk points, H_∂ the boundary points, and v and its transpose link boundary points to bulk points. This demarcation of the Hamiltonian naturally lends itself to a factorization of its determinant,

$$\det H = \det(H_\partial)\det(H/H_\partial), \tag{4.6}$$

where $H/H_\partial = (H_b - vH_\partial^{-1}v^T)$ is the Schur complement of H relative to H_∂. The importance of this term is that it encodes the precise correction to the bulk from the boundary layer.

Whereas H_b is manifestly local, the corrective piece $vH_\partial^{-1}v^T$ in the Schur complement couples nonlocal points. That is, given a point on the boundary which corresponds to some matrix element $(H/H_\partial)_{ii}$ its non-neighboring elements $(H/H_\partial)_{ii+2}, (H/H_\partial)_{ii+3}, \ldots$ are nonzero. Now, before integrating out the $(L+1)$th layer, all points strictly have nearest-neighbor links, so one boundary point will only be linked to its two boundary neighbors and the nearest-neighbor bulk points. Moreover, the two-point function for a particle propagating along the boundary is given by $G_{\partial\partial} \propto (1-\cos\theta)^{-\Delta}$. Consequently, we expect the non-locality arising from integrating out the extra layer to be suppressed as a function of the geodesic distance. Indeed, as Fig. 10 shows, by picking a boundary point and looking at its coupling to other boundary points, this nonlocal effect decays exponentially in geodesic distance.

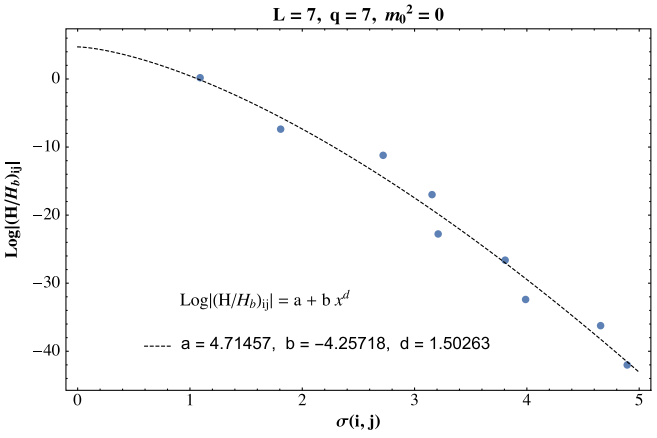

FIG. 10. The value of the matrix element of a chosen boundary point i in the Schur complement H/H_∂ and its boundary neighbors j. The exponential decay signals the vanishingly small coupling between nonlocal boundary points as a result of adding a new layer.

In summary we have shown that for any lattice size L we understand precisely how the $L+1$ layer corrects the Hamiltonian and that this correction preserves locality, so we can view our lattice as a local, low-energy effective theory obtained by integrating out layers from the $L \to \infty$ continuum.

V. FINITE LATTICE SPACING REFINEMENT

So far we have looked at the pure equilateral triangle group tessellation as an approximation of the hyperbolic plane. Relative to the continuum this introduces a finite lattice spacing error, with (2,3,7) triangles having a minimum spacing of $a \simeq 1.091$ relative to the fixed curvature length ℓ. The finite element approach to partial differential equations uses a sequence of nearly regular smaller simplices (triangles in 2d) when properly constructed allowing one to converge to exact continuum solutions, or in the context of quantum field theory to the classical tree approximation. Loops introduce UV divergences [24] but are neglected in our current presentation.

The linear interpolated finite elements method in 2d flat space for the Laplace Beltrami operator is equivalent to the method of discrete exterior calculus (DEC) [21]. The formal expression for the DEC Laplace-Beltrami operator acting on scalar fields in d-dimensions is $(\boldsymbol{\delta}+\mathbf{d})^2\phi = (\mathbf{d}\boldsymbol{\delta}+\boldsymbol{\delta}\mathbf{d})\phi = *\mathbf{d}*\mathbf{d}\phi$, with

$$\begin{aligned} *\mathbf{d}*\mathbf{d}\phi(i) &= \frac{|\sigma_0(i)|}{|\sigma_0^*(i)|}\sum_{j\in\langle i,j\rangle}\frac{|\sigma_1^*(ij)|}{|\sigma_1(ij)|}(\phi_i-\phi_j) \\ &= \frac{1}{\sqrt{g_i}}\sum_{j\in\langle i,j\rangle}\frac{S_{ij}}{l_{ij}}(\phi_i-\phi_j) \end{aligned} \tag{5.1}$$

in terms of the discrete exterior derivative $\mathbf{d}$ and its dual $\boldsymbol{\delta} = *d*$. The notation σ_n identifies a $n-$dimensional simplex[3] `points, lines, triangles`, etc. for $n = 0, 1, \ldots, d$ and $|\sigma_n^*|$ the $d-n$ dual polyhedron. $|\cdots|$ is the volume for these polyhedra. By convention $|\sigma_0(i)| = 1$. This coincides with the natural form of the divergence as a flux, where S_{ij} is the volume of the dual normal. To be concrete, in Fig. 3 (where $l_{ij} = |\sigma_1(ij)|$ is also indicated), S_{ij} is the length of the link $l_{ij}^* = |\sigma_1^*(ij)|$.

On our hyperbolic manifold it is natural and convenient to replace l_{ij} and l_{ij}^* by the appropriate geodesic lengths as

[3]More precisely, $\sigma_n(i_0, i_1, \cdots i_n)$ is the volume form for the n-simplex with vertices $i_0, i_1, \cdots i_n$ with value $\pm|\sigma_n|$ for even/odd permutations of the indices. See Ref. [21] for details.

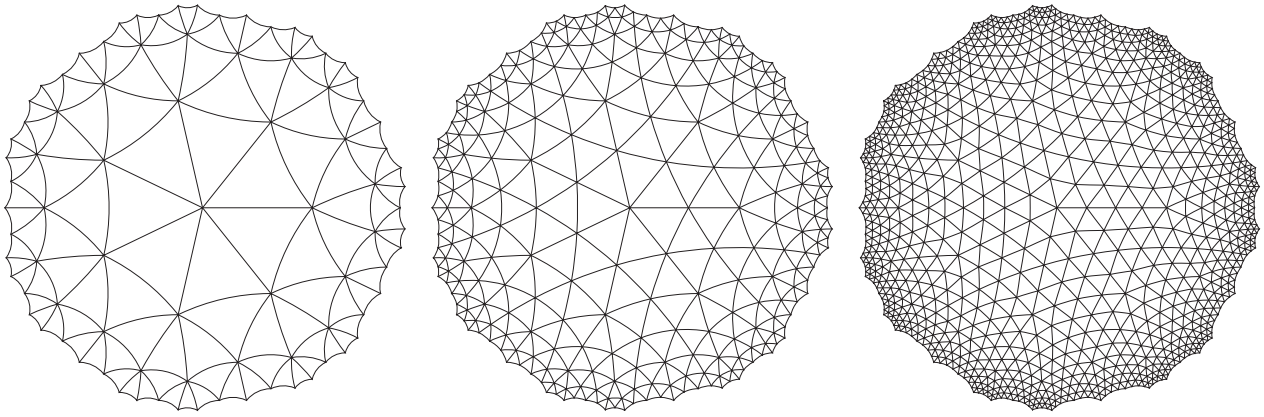

FIG. 11. Refinement of the $L = 3$, $q = 7$ lattice. The lattice is unrefined on the left, has one refinement in the middle, and two refinements on the right.

we have already been using this intrinsic geometry for the triangle group. To do this we need Heron's hyperbolic triangle area rule and the circumradius [25],

$$A(a,b,c) = 4\arctan\left[\sqrt{\tanh\frac{s}{2}\tanh\frac{s-a}{2}\tanh\frac{s-b}{2}\tanh\frac{s-c}{2}}\right]$$
$$R(a,b,c) = \operatorname{arctanh}\left[\left(\tanh\frac{a}{2}\tanh\frac{b}{2}\tanh\frac{c}{2}\right)\Big/\sin\frac{A(a,b,c)}{2}\right], \tag{5.2}$$

for a general hyperbolic triangle $\Delta(a, b, c)$ in terms of the side lengths a, b, c, with $s = (a + b + c)/2$. Finally, using the Pythagorean theorem for a hyperbolic right triangle, $\cosh(c) = \cosh(a)\cosh(b)$, we can solve for the length of the dual[4] from a side a into the triangle a, b, c—denoted $l^*(a, b, c)$—as

$$l^*(a,b,c) = \operatorname{arccosh}[\cosh R(a,b,c)/\cosh(a/2)]. \tag{5.3}$$

The above formulas allow us to calculate the weights l^*_{ij}/l_{ij} on an arbitrary lattice.

For the first iteration of this hyperbolic refinement we split our fundamental equilateral triangle into four subtriangles by bisecting each edge to half the lattice spacing: $a \to a/2$. The price we pay is a breaking of the $\mathbb{Z}_7$ symmetry at this scale so the subtriangles are neither equilateral nor congruent to each other. This means the FEM weights are no longer uniform.

Explicitly, the equilateral triangle at one refinement is split into three triangles of side lengths $(a/2, a/2, c)$ and one with sides (c, c, c), where for $q = 7$

$$a = 2\operatorname{arccosh}\left[\cos\frac{\pi}{3}\Big/\sin\frac{\pi}{7}\right] \approx 1.091,$$
$$c = \operatorname{arccosh}\left[\cosh^2\frac{a}{2} - \sinh^2\frac{a}{2}\cos\frac{2\pi}{7}\right] \approx 0.492. \tag{5.4}$$

Using (5.3) we find the kinetic weight l^*_{ij}/l_{ij} between two points i and j, which, is the factor K_{ij} in (2.6). For a single refinement there are only two different weights, one for those links that are already present in the original lattice (left image in Fig. 11), and another for those that are new in the refined lattice (middle image in Fig. 11). These two weights are

$$K_{\text{ij,orig}} = \frac{2l^*(\frac{a}{2},\frac{a}{2},c)}{a/2} = 0.490,$$
$$K_{\text{ij,ref}} = \frac{l^*(c,c,c) + l^*(c,\frac{a}{2},\frac{a}{2})}{c} = 0.643. \tag{5.5}$$

Note that for $K_{\text{ij,ref}}$, the length l^*_{ij} is the sum of two different lengths, one for the normal in each direction.

The rightmost image in Fig. 11 shows an example of a lattice refinement for two refinements. In principle this process can be applied recursively an arbitrary number of times. For the case of a lattice with a finite number of layers, in the limit of an infinite number of refinements we recover the continuum theory with a cutoff. More concretely, observables such as the bulk-to-bulk propagator that are sensitive to short distances in the bulk become closer to their continuum values as we add more refinements. Figure 12 shows this is indeed the case. We emphasize that Fig. 12 also shows that by using the correct boundary conditions, the unrefined triangle group lattice—even with a modest number of layers—produces remarkably accurate results.

[4]The "dual from a side a into the triangle a, b, c" means the segment from the center of a to the circumcenter of triangle a, b, c.

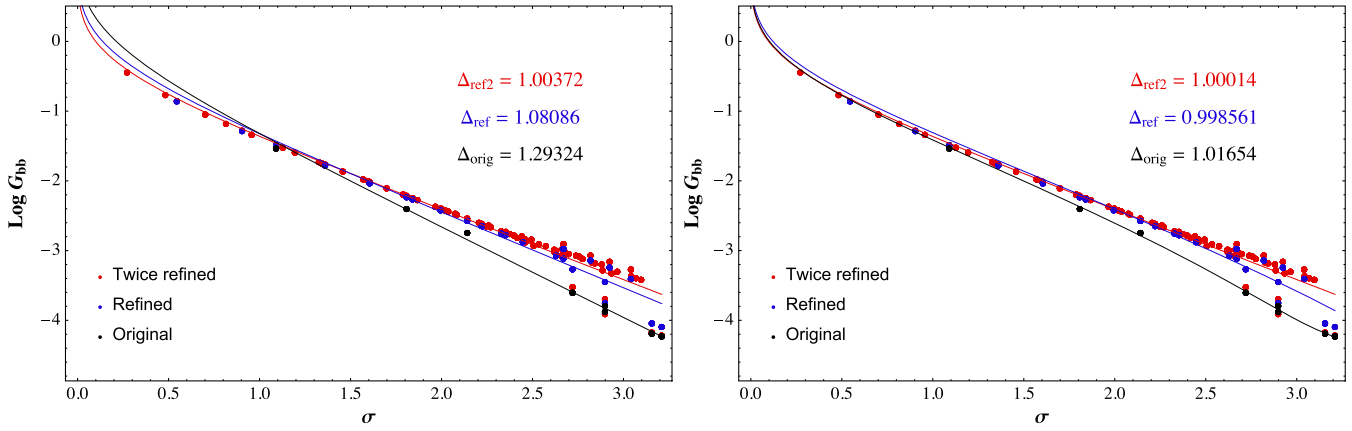

FIG. 12. The bulk-to-bulk propagator from a central source to all other points for the massless $L = 3$, $q = 7$ unrefined, once refined, and twice refined lattice, respectively. The fit for Δ is derived from the infinite BC corresponding to (3.2) for the left figure and solving the exact equation for a finite BC on the right.

VI. FUTURE DIRECTIONS

We have presented a triangulation of AdS_2 in order to establish a framework for nonperturbative lattice field theory methods on the hyperbolic disk $\mathbb{H}^2$. The $D(2,3,q)$ triangle group generates a lattice of equilateral triangles that preserve an exact discrete subgroup of the isometries. The case $q = 7$ gives the minimum area triangulation with a lattice spacing a that is $\mathcal{O}(1)$ in units of the curvature $K = 1/\ell^2$. Nonetheless, when introducing ϕ^4 theory we find remarkably good comparisons for propagators, the tree-level four-point amplitude, and the Laplacian eigenspectrum on a Poincaré disk of finite geodesic radius. We also introduce methods to reduce the lattice spacing by application of finite elements refinement using discrete exterior calculus. We propose that this initial lattice is sufficient for a first semiquantitative, nonperturbative investigation of the AdS_2/CFT correspondence in the limit that gravity is decoupled.

We have restricted our attention to a scalar field theory in AdS_2 for simplicity, but it would be interesting to generalize to a wider class of field theories. The inclusion of bulk Abelian and non-Abelian gauge theories and Dirac Fermions should be straightforward following the approach of Ref. [18] for de Sitter. Kähler Dirac fermions are naturally adapted to simplicial lattices using DEC as described in Ref. [26]. Generalizing to higher dimensions should also be possible, and it is an interesting question what constitutes the best choice for lattices on higher dimensional AdS.

Ultimately, the point is to eventually do nonperturbative Monte Carlo lattice simulations of bulk field theories, and compute correlators in the dual boundary CFTs. A natural first effort is to study $\lambda\phi^4$ theory AdS_2 at strong coupling. In that case, one could compare results for the spectrum of the dual CFT_1 to constraints from the conformal bootstrap [27].

We also note that hyperbolic graphs are playing an increasingly prominent role in other applications such as tensor networks [5–7] and quantum error correction codes [8,9]. These networks are employed in the computation of entanglement entropies [28] for boundary field theories. For this reason, our sketch of the triangle group algebra may have relevance beyond the present context.

ACKNOWLEDGMENTS

We would like to thank Simon Catterall for enlightening and helpful discussions. A. L. F. and R. C. B. were supported in part by the U.S. Department of Energy Office of Science under Award No. DE-SC0015845. A. L. F. was supported in part by a Sloan Foundation fellowship. This work was supported in part by the U.S. Department of Energy (DOE) under Award No. DE-SC0019139.

APPENDIX A: HYPERBOLIC PLANE

In this Appendix we reproduce various results of the hyperbolic plane.

1. Metric

There are various forms of the metric:

$$ds^2 = \ell^2(d\rho^2 + \sinh^2\rho d\theta^2) \quad \text{(Geodesic coordinates)} \quad \text{(A1)}$$

$$= \frac{4\ell^2}{(1-r^2)^2}(dr^2 + r^2 d\theta^2) \qquad \left(\text{Global coordinates: } r = \tanh\frac{\rho}{2},\ \rho = \log\frac{1+r}{1-r}\right) \tag{A2}$$

$$= 4\ell^2 \frac{dzdz^*}{(1-|z|^2)^2} (\text{Poincaré disk: } z = re^{i\theta}) \tag{A3}$$

$$= \ell^2 \frac{dwdw^*}{(\text{Im}w)^2} \left(\text{Upper-half plane: } z = \frac{w-i}{w+i}\right) \tag{A4}$$

$$= \ell^2 \frac{dx^2 + dy^2}{y^2} (\text{Upper-half plane: } w = x + iy) \tag{A5}$$

$$= \ell^2(-dX_0^2 + dX_1^2 + dX_2^2) \qquad (\text{Embedding Space: } X_0 = \cosh\rho, X_1 \pm iX_2 = e^{\pm i\theta}\sinh\rho) \tag{A6}$$

The chordal distance

$$d_{\text{ch}}(X, X') \equiv -\frac{1}{2}(X - X')^2 \equiv \ell^2\left(1 - \frac{1}{\xi(X, X')}\right), \qquad \xi(X, X') \equiv -\frac{\ell^2}{X \cdot X'}, \tag{A7}$$

is related to the geodesic distance (in units of AdS radius ℓ) $\sigma(X, X')$ by

$$\cosh(\sigma) = \frac{1}{\xi} \leftrightarrow \sigma = \log\left(\frac{1 + \sqrt{1-\xi^2}}{\xi}\right), \tag{A8}$$

as is easily verified by evaluating the chordal distance in geodesic coordinates between the point at $\rho = 0$ and any other point. The embedding space coordinates are related to the UHP coordinates by

$$X_0 = \frac{1 + x^2 + y^2}{2y}, \qquad X_1 = \frac{-1 + x^2 + y^2}{2y}, \qquad X_2 = -\frac{x}{y}, \tag{A9}$$

from which one can easily obtain

$$\xi(X, X') = \frac{2yy'}{(x - x')^2 + y^2 + y'^2}. \tag{A10}$$

Lastly, we also mentioned that, for the Poincaré disk, the geodesic distance between two points z and z' can be expressed as

$$\sigma(z, z') = 2\tanh^{-1}\left|\frac{z - z'}{1 - z^* z'}\right|. \tag{A11}$$

2. Hyperbolic trigonometry

Now we turn to triangles, with interior angles (α, β, γ) with opposite geodesic side lengths of (a, b, c) in units of curvature $\ell = 1$. We will be primarily interested in the case of negative constant curvature, where $\alpha + \beta + \gamma < \pi$. The triangle area A_Δ is given by (2.4), with ratios for its sides fixed. For equilateral triangles, $\alpha = \beta = \gamma$ and $a = b = c$, one has

$$\cosh a/2 = \frac{1}{2\sin\alpha/2}. \tag{A12}$$

In this paper we are interested primarily in equilateral triangles with $\alpha = \beta = \gamma = \frac{2\pi}{q}$ and $q = 7, 8, \ldots$, thus

$$a = 2\cosh^{-1}\frac{1}{2\sin\pi/q}. \tag{A13}$$

For right triangles with $\gamma = \pi/2$,

$$\cosh a = \frac{\cos\alpha}{\sin\beta}, \quad \cosh c = \frac{\cos\beta}{\sin\alpha}, \quad \cosh c = \cot\alpha\cot\beta. \tag{A14}$$

The last relation corresponds to the Pythagorean theorem. In particular, consider $(\alpha, \beta, \gamma) = (\frac{\pi}{2}, \frac{\pi}{3}, \frac{\pi}{q})$. For the side opposite the angle $\beta = \pi/3$,

$$b = \cosh^{-1}\frac{\cos\pi/3}{\sin\pi/q} = \cosh^{-1}\frac{1}{2\sin\pi/q} = a/2, \tag{A15}$$

where a above is the geodesic length for the side of the (q,q,q) equilateral triangle, given in (A13), and also in (2.10).

APPENDIX B: ACTION OF TRIANGLE GROUP ON THE LATTICE

The maximally symmetric lattices we use in this paper are irreducible representations of the proper $D(2,3,q)$ triangle group, so that every point in the lattice is related to every other point by a symmetry of the lattice. Here, we exhibit the action of this symmetry explicitly, in Poincaré disk complex coordinates $z = re^{i\theta}$ mapped from the UHP coordinates $w = x + iy$ by $z = (w-i)/(w+i)$. The symmetry of the continuum spacetime is $PSL(2,\mathbb{R})$, of which the triangle group is a discrete subgroup.

As discussed in Sec. II A, the triangle group $D(p,r,q)$ is generated by two elements S and T satisfying

$$S^p = 1, \qquad T^r = 1, \qquad U^q = 1, \qquad U = ST. \tag{B1}$$

We are interested in the case $(p,r,q) = (2,3,q)$ so that six triangles with angles $(\frac{\pi}{2},\frac{\pi}{3},\frac{\pi}{q})$ form a cell of an equilateral triangle, as illustrated in Fig. 1, and our lattice is the vertices of these equilateral triangles. We will orient our lattice so that one vertex is at the center $z = 0$ in Poincaré disk coordinates, and a neighboring vertex is along the positive real axis as in Fig. 3. The action of U on the lattice is just a rotation by $2\pi/q$:

$$U : z \to e^{2\pi i/q} z. \tag{B2}$$

Using the map $z = \frac{w-i}{w+i}$ from the Poincaré disk to the UHP, it is easy to infer the action of U on the lattice in UHP coordinates. We can represent this action as an element of $PSL(2,\mathbb{R})$ as follows:

$$U : w \to \frac{aw+b}{cw+d}, \qquad \begin{pmatrix} a & b \\ c & d \end{pmatrix} = \begin{pmatrix} \cos\frac{\pi}{q} & -\sin\frac{\pi}{q} \\ \sin\frac{\pi}{q} & \cos\frac{\pi}{q} \end{pmatrix}. \tag{B3}$$

The action of S and T are more difficult to infer, but easy to check once they are known. For S, its action on the UHP is given by

$$S \cong \begin{pmatrix} 0 & b \\ -\frac{1}{b} & 0 \end{pmatrix}, \qquad b = e^{\operatorname{sech}^{-1}(2\sin\frac{\pi}{q})}. \tag{B4}$$

Clearly, $S^2 \cong 1$ in $PSL(2,\mathbb{R})$. The action of T is simply $T = US$, and one can check that $T^3 = (US)^3 \cong 1$.

Finally, we can translate the action of S on the UHP to its action on the Poincaré disk:

$$S : z \to \frac{z - \sqrt{2\cos(2\pi/q) - 1}}{\sqrt{2\cos(2\pi/q) - 1}\, z - 1}. \tag{B5}$$

As a check, note that S takes the origin in z-coordinates to $z_1 = \sqrt{2\cos(\frac{2\pi}{q})} - 1$. By (A.2), the geodesic distance between the origin and z_1 is $2\tanh^{-1}|z_1| = 2\cosh^{-1}\frac{1}{2\sin(\frac{\pi}{q})}$. This gives us an independent derivation for the length a of the edges of the lattice, which agrees with our previous formula (2.10). In terms of this geodesic length a, the transformation S can be seen as a boost

$$S : z \to \frac{\cosh(a/2)z - \sinh(a/2)}{\sinh(a/2)z - \cosh(a/2)}. \tag{B6}$$

Because the lattice is an irreducible representation of $D(2,3,q)$, one can generate the entire lattice by starting with one point and repeatedly acting with S and T. So for instance, if we take our initial point to the origin of the Poincaré disk, then acting with S generates one vertex of the first layer. Acting with T^n for $n = 0,\ldots,q-1$, this vertex is repeatedly rotated by $2\pi/q$ to fill out the rest of the first layer. Then, we can act with S again to generate points on the second layer, and acting multiple times with T to fill out the second layer, and so on.

APPENDIX C: RECURSIVE ENUMERATION ON THE TRIANGULATED DISK

The construction of our triangulated lattice on $\mathbb{H}^2$ is defined by recursively adding one layer at time starting from $r = 0$. Each layer has $n(L)$ vertices on a periodic ring connected by single links on the triangles between them. The total number of links between two layers is $n(L) + n(L-1)$. Consequently, one obtains a sum rule by counting the number of links (or *flux*) through each layer. Consider the number of vertices $n(L-1)$ at layer $L-1$. All the vertices must have exactly q neighbors. Of the q links (per vertex) to these neighbors, two are around the circumference of the layer, and $q-2$ must either enter from layer $L-2$ or exit to layer L. This gives the sum rule,

$$\begin{aligned}(q-2)n(L-1) \\ = [n(L) + n(L-1)] + [n(L-1) + n(L-2)],\end{aligned} \tag{C1}$$

or the two term recursion relation in (2.11),

$$n(L) = (q-4)n(L-1) - n(L-2). \tag{C2}$$

The solution is the sum of two homogeneous powers, $n(L) = c_+ x_+^L + c_- x_-^L$, where

$$x_\pm = 1/x_\mp = \frac{1}{2}\left[(q-4) \pm \sqrt{(q-6)(q-2)}\right] \tag{C3}$$

are the roots of the quadratic equation $x^2-(q-4)x+1=0$. To fix the coefficients $c_\pm$ we need two starting conditions. In our construction we chose the q-fold vertex at $r=0$, so the initial condition is $n(0)=0, n(1)=q$. So the particular the solution for our D(2,3,7) lattice is

$$n(L)=\frac{7}{\sqrt{5}}[(3/2+\sqrt{5}/2)^L-(3/2-\sqrt{5}/2)^L]. \quad \text{(C4)}$$

However, if we were to place a 3-fold circumcenter of the equilateral triangle at $r=0$, the initial condition would be $n(0)=3, n(1)=(q-4)n(0)$. An equivalent approach is to build both initial conditions into a generating function, $N(z)=\sum_{i=0}^{\infty} n(i)z^i=(n(0)+z(n(1)+(q-4)n(0)))/((z-x_+)(z-x_-))$, computing $n(L)=(2\pi i)^{-1}\oint dz z^{-1-L}\times N(z)$ by contour integration.

The total number of vertices in our D(2,3,q) disk is

$$V(q,L)=1+\sum_{i=1}^{L} n(i). \quad \text{(C5)}$$

By Euler's identity for a triangulated disk, $V-E+F=1$ (zero handles and one boundary) the number of edges (E) and faces (F) are also fixed. To include the boundary term, it is convenient to first add a point vertex at ∞, starting with Euler's identity for a triangulated sphere obeying $V_\circ-E_\circ+F_\circ=2-H=2$ and the constraint $2E_\circ=3F_\circ$. Then it is simple to solve these two equations for E_0 and F_0 in terms of V_0 to find $E_0=3V_0-6, F_0=2V_0-4$. Deleting the links between the $B(q,L)=n(L)$ boundary sites eliminates $B(q,L)$ edges and $B(q,L)$ faces, but only one vertex. Therefore the number of edges $E(q,L)$ and faces $F(q,L)$ in the disk with the point at infinity deleted are

$$\begin{aligned} E(q,L)&=3V(q,L)-3-B(q,L),\\ F(q,L)&=2V(q,L)-2-B(q,L), \end{aligned} \quad \text{(C6)}$$

where $V(q,L)$ is the number of vertices in the graph. One can easily check that (C6) solves the Euler identity on the disk.

Since all of these functions scale as x_+^L for large L, we can obtain rigorous scalings of our hyperbolic network toward the boundary. Assuming that the layers are on average spherical, a comparison is made between the area of the finite disk in the continuum,

$$A_{\text{disk}}=2\pi\int_0^{\rho_0} d\rho\sinh(\rho)=2\pi(\cosh(\rho_0)-1), \quad \text{(C7)}$$

and the area of the triangulated lattice

$$A_{\text{lat}}=A_\Delta(q)F(q,L)=(\pi-6\pi/q)F(q,L). \quad \text{(C8)}$$

Matching the exponential growth for $A_{\text{disk}}\sim A_{\text{lat}}$ we find that

$$\rho_0\simeq\log(x_+)L=\log[(q-4)/2+\sqrt{(q-6)(q-2)}/2]L, \quad \text{(C9)}$$

so that the effective lattice spacing between layers is

$$a_q=\log[(q-4)/2+\sqrt{(q-6)(q-2)}/2]. \quad \text{(C10)}$$

For $q=7$ the effective lattice spacing in ρ is $a_7=0.962424$, which is consistent with the numerical estimate, $\tilde{c}_7=0.919$, from the finite L extrapolation in (2.12).

With this identification of the lattice spacing the solution for general q is written,

$$n(L)=\frac{q}{2\sinh(a_q)}[e^{a_qL}-e^{-a_qL}]=\frac{q\sinh(a_qL)}{\sinh(a_q)}. \quad \text{(C11)}$$

The flat space limit, $q\to 6, a_q\to 0$, gives the correct enumeration, $n(L)=6L$, of vertices at each layer for the triangular lattice.

Several comments are worth making. First it is interesting to look at the q-dependence for $a_q=0.9624$, 1.317, 1.567 for $q=7$, 8, 9, respectively. Remarkably this is the same lattice spacing $b=0.96$, 1.34, 1.66 determined numerically in Sec. III C by fitting to the Green's function for large AdS mass.

Next we note this recursive enumeration is general for any triangulated planar graph. Starting from a node, each layer is defined by single link to the next layer. Consequently this can be applied to the coarse graining of an ensemble of Regge calculus triangulations approximating a smooth manifold with small average values of $\langle q-6\rangle\simeq 0$. To this end, rewrite the recursion relation as

$$n[L+1]-2n[L]+n[L-1]=(q-6)n[L], \quad \text{(C12)}$$

which approaches the following continuum equation,

$$\partial_\rho^2 n(\rho)\simeq\frac{(q-6)}{a_q^2}n(\rho), \quad \text{(C13)}$$

in the limit with $a_q\simeq\sqrt{q-6}$ as $\langle q\rangle\to 6$. So for $\rho\gg a_q$ the continuum solution $n(\rho)\sim e^\rho$ gives precisely the right exponential growth in arc length in θ for AdS_2 at fixed ρ. Similar methods would also apply to our DEC refinement scheme as it approaches the continuum.

[1] D. Carmi, L. Di Pietro, and S. Komatsu, A study of quantum field theories in AdS at finite coupling, J. High Energy Phys. 01 (2019) 200.

[2] O. Aharony, M. Berkooz, D. Tong, and S. Yankielowicz, Confinement in anti-de Sitter space, J. High Energy Phys. 02 (2013) 076.

[3] O. Aharony, D. Marolf, and M. Rangamani, Conformal field theories in anti-de Sitter space, J. High Energy Phys. 02 (2011) 041.

[4] O. Aharony, M. Berkooz, and S.-J. Rey, Rigid holography and six-dimensional $\mathcal{N} = (2, 0)$ theories on $AdS_5 \times \mathbb{S}^1$, J. High Energy Phys. 03 (**2015**) 121.

[5] G. Evenbly, Hyperinvariant Tensor Networks and Holography, Phys. Rev. Lett. **119**, 141602 (2017).

[6] A. Jahn, M. Gluza, F. Pastawski, and J. Eisert, Holography and criticality in matchgate tensor networks, Sci. Adv. **5**, eaaw0092 (2019).

[7] L. Boyle, B. Dickens, and F. Flicker, Conformal Quasicrystals and Holography, Phys. Rev. X **10**, 011009 (2020).

[8] B. Swingle, Entanglement renormalization and holography, Phys. Rev. D **86**, 065007 (2012).

[9] A. Almheiri, X. Dong, and D. Harlow, Bulk locality and quantum error correction in AdS/CFT, J. High Energy Phys. 04 (2015) 163.

[10] A. J. Kollár, M. Fitzpatrick, and A. A. Houck, Hyperbolic lattices in circuit quantum electrodynamics, Nature (London) **571**, 45 (2019).

[11] I. Boettcher, P. Bienias, R. Belyansky, A. J. Kollár, and A. V. Gorshkov, Quantum simulation of hyperbolic space with circuit quantum electrodynamics: From graphs to geometry, Phys. Rev. A **102**, 032208 (2020).

[12] H. S. M. Coxeter and W. O. J. Moser, *Generators and Relations for Discrete Groups* (Springer-Verlag, Berlin, 1980).

[13] S. Levy, *The Eightfold Way: The Beauty of Klein's Quartic Curve* (Cambridge University Press, Cambridge, England, 2001).

[14] H. P. de Saint-Gervais, *Uniformization of Riemann Surfaces: Revisiting a Hundred-Year-Old Theorem* (European Mathematical Society, Zürich, 2010).

[15] G. Jones and J. Wolfart, *Dessins d'Enfants on Riemann Surfaces* (Springer-Verlag, Berlin, 2016).

[16] D. Mumford, C. Series, and D. Wright, *Indra's Pearls: The Vision of Felix Klein* (Cambridge University Press, Cambridge, England, 2002).

[17] G. Strang and G. Fix, *An Analysis of the Finite Element Method*, 2nd ed. (Wellesley-Cambridge, 2008), http://amazon.com/o/ASIN/0980232708/.

[18] R. C. Brower, E. S. Weinberg, G. T. Fleming, A. D. Gasbarro, T. G. Raben, and C.-I. Tan, Lattice Dirac fermions on a simplicial Riemannian manifold, Phys. Rev. D **95**, 114510 (2017).

[19] R. C. Brower, M. Cheng, E. S. Weinberg, G. T. Fleming, A. D. Gasbarro, T. G. Raben, and C.-I. Tan, Lattice ϕ^4 field theory on Riemann manifolds: Numerical tests for the 2-d Ising CFT on $\mathbb{S}^2$, Phys. Rev. D **98**, 014502 (2018).

[20] N. H. Christ, R. Friedberg, and T. D. Lee, Weights of links and plaquettes in a random lattice, Nucl. Phys. **B210**, 337 (1982).

[21] M. Desbrun, A. N. Hirani, M. Leok, and J. E. Marsden, Discrete exterior calculus, arXiv:math/0508341.

[22] C. P. Burgess and C. A. Lutken, Propagators and effective potentials in anti-de sitter space, Phys. Lett. **153B**, 137 (1985).

[23] E. Hijano, P. Kraus, E. Perlmutter, and R. Snively, Witten diagrams revisited: The AdS geometry of conformal blocks, J. High Energy Phys. 01 (2016) 146.

[24] R. C. Brower, M. Cheng, E. S. Weinberg, G. T. Fleming, A. D. Gasbarro, T. G. Raben, and C.-I. Tan, Lattice ϕ^4 field theory on riemann manifolds: Numerical tests for the 2d ising cft on $\sim^2$, Phys. Rev. D **98**, 014502 (2018).

[25] Á. G. Horváth, On the hyperbolic triangle centers, in *Studies of the University of Zilina*, Math. Series (2015), p. 11.

[26] S. Catterall, J. Laiho, and J. Unmuth-Yockey, Kähler-Dirac fermions on Euclidean dynamical triangulations, Phys. Rev. D **98**, 114503 (2018).

[27] M. F. Paulos, J. Penedones, J. Toledo, B. C. van Rees, and P. Vieira, The S-matrix bootstrap. Part I: QFT in AdS, J. High Energy Phys. 11 (2017) 133.

[28] H. Yan, Hyperbolic fracton model, subsystem symmetry, and holography, Phys. Rev. B **99**, 155126 (2019).